Journal of Crystal Growth 533 (2020) 125469

Contents lists available at ScienceDirect

Journal of Crystal Growth

journal homepage: www.elsevier.com/locate/jcrysgro

On the thermal stability of nearly lattice-matched AlInN films grown on GaN via MOVPE

Damir Borovac*, Wei Sun, Renbo Song, Jonathan J. Wierer Jr., Nelson Tansu

Center for Photonics and Nanoelectronics, Department of Electrical and Computer Engineering, Lehigh University, Bethlehem, PA 18015, USA

ARTICLE INFO

Communicated by G.B. Stringfellow

Keywords:
A1. X-ray diffraction
A1. Atomic force microscopy
A2. Single crystal growth
A3. Metalorganic vapor phase epitaxy
B1. Nitrides
B2. Semiconducting materials

ABSTRACT

The thermal stability of nearly lattice-matched AlInN films grown via metalorganic vapor phase epitaxy on GaN/sapphire is investigated. The structural and morphological changes of the AlInN layers, as determined by x-ray diffraction (XRD) and atomic force microscopy (AFM), are studied when systematically varying annealing times, temperatures, and ambients to gain a better understanding of the temperature limits of the AlInN films. The samples are annealed either in the growth chamber with the same conditions (gases, pressure, and flow rates) as the original growth conditions of the AlInN samples, or in the XRD under N_2. In general, the surface of the AlInN changes at temperatures > 850 °C under growth and N_2 conditions mostly likely due to a loss of In as determined by AFM. However, the bulk crystal structure of the AlInN remains stable up to temperatures of 950–1050 °C (depending on ambient) as determined by XRD. These findings provide a helpful guide for future experiments involving high-temperatures (790–1050 °C) for subsequent or transition layers during epitaxial growth, and for fabricating device structures employing AlInN layers.

1. Introduction

III-nitride semiconductors have gained tremendous attention due to their favorable optoelectronic [1], chemical [2], tribological [3] and other advantageous material properties that make them an excellent candidate for a variety of applications [4–7]. In addition to their successful implementation in solid-state lighting, III-nitride semiconductors are also being using in next-generation power devices, with examples of GaN-based devices already replacing some Si-based power devices [8]. Beyond GaN for power electronics devices are ultrawide bandgap (UWBG) semiconductors, such as β-Ga_2O_3, AlGaN, and BN. Interest in these semiconductors has increased dramatically, owing to the potential of achieving high temperature, high electric field, high breakdown voltage operations, along with a high power figure-of-merit (FOM). However, realizing UWBG power devices is difficult because of challenges such as the lack of p-type doping for β -Ga_2O_3 or substrates for high Al content AlGaN [8].

Within the same UWBG range is AlInN which possesses most of the necessary requirements to create a wide array of power electronics devices, including a high energy bandgap (~4.4 eV) [9], lattice-matched substrates to GaN with In/Al ratio of 17:83 [12], p- and n-type doping [10,11], and the ability to oxidize thick layers [13]. The usage of AlInN has been explored for several other applications, including high-electron-mobility transistors (HEMTs) [14,15], distributed Bragg reflectors (DBRs) [9], integration as an electron barrier layer in InGaN-based quantum wells [16], thermoelectricity [17], and Schottky photodiodes for ultraviolet detection [18]. In our recent work we proposed the use of AlInN for vertical power devices [19]. Additionally, our recent efforts on optimizing growth conditions have produced AlInN films with extremely low background electron concentrations (n) of ~10^{17} cm^{-3} [20]. Certainly, lower n will also aid in increasing p-type doping (hole concentration) in AlInN alloys. Thus, by utilizing advances in III-nitride epitaxy and incorporating extensive innovations in device design, AlInN is an excellent candidate for applications such as power electronic devices and deep-ultraviolet light-emitting diodes (LEDs).

Exposure of AlInN to temperatures above their typical growth temperature (~800 °C) has been investigated by several groups, typically with the aim to understand optimal growth sequencing, and thereby the interface quality, to achieve extremely high reflectivity (> 99%) distributed Bragg reflectors using alternating AlInN and GaN layers [21–23]. Due to the vastly different growth conditions (temperature, pressure, V/III ratio and ambient gases) used in AlInN and GaN epitaxy, it is very important to carefully adjust the growth sequence when transitioning from one layer (AlInN) to another (GaN). The work by Carlin et al. [21] served as a catalyst to understand the influence of various growth schemes to obtain high-quality AlInN/GaN

* Corresponding author.
E-mail addresses: dab315@lehigh.edu (D. Borovac), tansu@lehigh.edu (N. Tansu).

https://doi.org/10.1016/j.jcrysgro.2019.125469
Received 23 October 2019; Received in revised form 22 December 2019; Accepted 27 December 2019
Available online 28 December 2019
0022-0248/

interfaces [22–28]. Although Refs. [21–23] suggest that the growth of high temperature GaN does not degrade the surface morphology and interface quality of the AlInN/GaN layers, others have pointed out the non-triviality of such epitaxy. For example, Sadler et al. [25] demonstrated that a GaN capping layer is necessary to preserve the quality of ~50 nm thick AlInN films and obtain smooth surfaces, and Berger et al. [27] surmised that a thin (~2 nm) AlN interlayer may be formed due to indium (In) desorption when a GaN capping is not used. Moreover, Gadanecz et al. [29] investigated the thermal stability of AlInN with various In-content and determined that lattice-matched $In_xAl_{1-x}N$ ($x \sim 0.174$) samples are stable for temperatures up to 960 °C, while non-lattice-matched samples exhibited severe loss of indium even at temperatures below their respective growth temperatures (i.e. 400 °C). However, these past reports on the structural and surface-related properties of AlInN exposed to high temperatures are broad in their temperature analysis, and only provide a wide range of acceptable temperatures where the semiconductor is stable. In this paper, a rigorous analysis is undertaken to quantify the temperatures dictating the thermal limits of AlInN. Understanding the thermal limits is useful for metalorganic vapor phase epitaxy (MOVPE) growth of AlInN to ensure uncompromised surfaces and crystal quality.

In this work, investigation of the thermal stability of nearly-lattice-matched $Al_xIn_{1-x}N$ films ($x \sim 0.83$) grown via MOVPE on top of GaN on sapphire templates is demonstrated. The materials studied here are grown at a higher growth pressure (75 Torr) and have low as-grown surface roughness in comparison to earlier studies (20 Torr) [12]. The changes of the surface morphology and structural characteristics of the annealed samples are studied by means of atomic force microscopy (AFM) and X-ray diffraction (XRD). The discussion is split into three different sections. *Section I* focuses on varying the annealing temperature from 790 °C to 1030 °C for ~ 75 nm thick AlInN samples (S1) placed back into the growth chamber (GC) with similar conditions to AlInN growth (GC anneal), and with an annealing time of 1 min. In Section II, ~75 nm thick AlInN samples (S2) are subjected to temperatures of 850 °C, 950 °C and 1050 °C with a GC anneal for 120 min to understand the limit of the sample quality when exposed to annealing for longer times. *Section II* also includes findings on XRD measurements performed with various anneals inside the XRD system (XRD anneal) at temperatures up to 1050 °C to evaluate the recoverability of samples exposed to thermal cycling in an N_2 atmosphere. *Section III* contains the findings on "thick" (~275 nm) AlInN samples (S3) exposed to a GC anneal at 1050 °C at various times, ranging from 15 min up to 120 min to understand the stability at typical GaN growth temperatures. Thus, this work serves as a guide for future growth and device processing of AlInN films nearly-lattice-matched to GaN with various thicknesses that require temperatures above the typical growth temperature of AlInN.

2. Experimental and methods

The X-ray diffraction measurements are performed using a PANalytical Empyrean X-ray diffraction system, equipped with a Ge (2 2 0) hybrid monochromator with Cu $K\alpha_1$ x-rays ($\lambda = 1.540598$ Å) as the light source and a PIXcel 3D detector. The AFM images are taken using a Veeco Dimension 5000. The alloy compositions are determined by using symmetric XRD scans in the (0 0 2) direction and fitting the scans with the PANalytical X'Pert Epitaxy software. Additionally, an analysis using $\omega/2\theta$ scans in the (0 0 2) and (1 0 $\bar{1}$ 5) directions is performed to determine the lattice parameters and alloy compositions, assuming a linear interpolation using Vegard's law, and lattice parameters of AlN and InN (assuming no isotropic strain in the c-plane). These values are then corrected similar to the case of AlGaN [30], with a Poisson ratio of $\upsilon = 0.36$, and is found to be in very good agreement from what is obtained with the X'Pert Epitaxy software. It should also be noted that throughout this study we used the values of the full-widths at half-maximum (FWHM) from the XRD measurements as a means to quantify the broadening stemming from potential crystallographic changes occurring in the AlInN crystal, to which we refer to as crystalline quality and crystalline stability throughout the manuscript. The values of FWHM can provide an indicative representation of whether there are changes occurring to the AlInN crystal, but studies depicting the exact physical mechanisms governing these changes will be reserved for future studies.

The thermal treatments performed in this study are separated in two different categories, where the GC anneal is performed inside the reactor chamber using the same conditions (gases, pressure and flow rates) as the original growth conditions of the AlInN samples, except without any metalorganic (MO) source flow. The second type of annealing is the XRD anneal which is performed inside the PANalytical Empyrean XRD system using a domed hot stage to control the atmosphere with a constant supply of N_2.

The AlInN samples are grown by MOVPE in a vertical-flow Veeco P-75 reactor. The group-V precursor is ammonia (NH_3), and the group-III precursors are trimethylindium (TMIn) and trimethylaluminum (TMAl). All AlInN epitaxial films are grown on n-type GaN ($n \sim 5 \times 10^{18}$ cm^{-3}) templates (formed on top of patterned-sapphire substrate) at a pressure of 75 Torr and N_2 as the carrier gas. The AlInN samples in this study are labeled as S1, S2 and S3 and the numbers are linked to their respective sections in this manuscript. The source flow rates are adjusted to produce a TMIn / TMAl molar flow ratio of ~ 1.65. Then, the growth temperatures of the three samples are vary slightly from 790 °C (S1), to 795 °C (S2) and 785 °C (S3), and result in In-contents are nearly lattice matched at 17.2%, 18.2% and 16.9%, respectively. The growth rates are estimated to be around 2.5 nm/min for all the samples presented and are determined by using spectroscopic ellipsometry (SE), X-ray reflectivity (XRR), and the reflectivity traces generated during the growth (data not shown).

3. Section I – Short time annealing study of AlInN

In this section, the results of a series of GC anneals for 1 min at different temperatures on the AlInN samples (S1) are presented. This experiment provides essential clues on the limit of the thermal stability of AlInN when exposed to temperatures above the typical growth temperature (~790 °C). It will help precisely optimize the growth temperature of layers subsequent to AlInN layers. Thus, the annealing time (1 min) is chosen to closely resemble that of a typical transition layer during growth. It should be noted that for this experiment it is assumed any memory effects from the chamber will not produce any significant changes to the sample surface or overall crystalline quality during the annealing process, and that the ramping time for all annealing steps is kept constant.

Fig. 1(a) shows the $\omega/2\theta$ (0 0 2) scans for the S1 samples annealed inside the GC for 1 min at temperatures varying from 790 °C up to 1030 °C. The vertical dashed lines in Fig. 1(a) are plotted used to highlight potential changes in the location of the GaN or AlInN peaks obtained during the XRD scans. No significant peak shifts for the AlInN can be observed for any of the annealing temperatures, indicating the overall high crystalline stability of the S1 sample when exposed to temperatures up to 1030 °C. Moreover, no additional AlInN-related peaks can be observed, suggesting that phase separation or significant loss of the cations (Ga or In) has not occurred within the detection of the XRD setup. This is similar to observations made by Gadanecz et al. [29] for the case of pseudomorphically grown AlInN, but they also noted that AlInN films deviating from the lattice-matched conditions will undergo significant changes even at temperatures of 400 °C [29]. Additionally, Gadanecz et al. suggested that strong melt back etching prevented annealing studies above 960 °C, which is not observed in this work, and therefore allowed for a larger window of annealing temperatures to be investigated. The as-grown samples presented here have AlInN XRD spectra with full-widths at half-maximum (FWHM) that are approximately 4 times lower than Ref. [29], and the improved temperature stabililty could be a result of higher crystallinity.

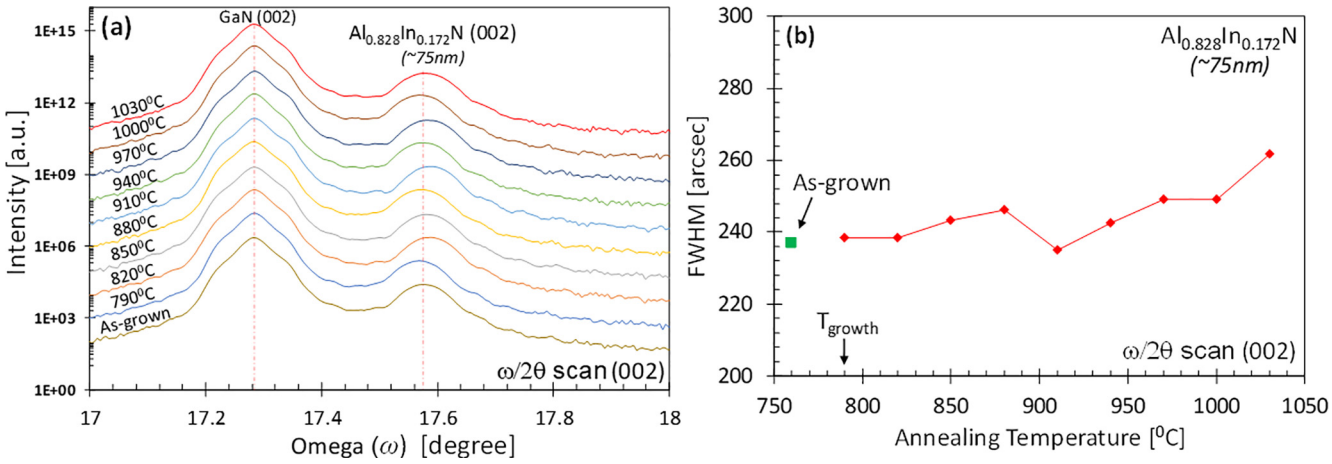

Fig. 1. (a) XRD ω/2θ (0 0 2) scans of S1 samples annealed for 1 min at varying temperatures in the reactor chamber and (b) FWHM as a function of annealing temperature obtained from the ω/2θ (0 0 2) scans.

A qualitative measure of the overall crystalline quality and stability of the "main" AlInN films can be investigated through analyzing the FWHMs of the annealed samples, as shown in Fig. 1(b). Here, the "main" part of the film is defined as the bulk of the AlInN layer and not necessarily the top-most surface, as the XRD scans results in an averaging effect as the x-rays sample the entire AlInN layer. In Fig. 1(b) the FWHM of the S1 samples for temperatures up to 1000 °C show no significant increase (~5%). However, at an annealing temperature of 1030 °C the FWHM increases by ~10%. This widening of FWHM suggests changes in the AlInN film with a possibility of reconstruction at the surface is taking place which can be attributed to desorption of indium from the surface, as has been suggested by others [25–26,28]. Thus, the growth temperature of layers subsequent to AlInN should be at or below 1000 °C in order to preserve the quality of the AlInN layer. For example, avoiding crystal degradation of AlInN is useful to minimize the variations in the refractive indices at the interfaces between AlInN and GaN in DBR layers to producing precise reflectivity spectra.

Fig. 2(a)–(d) show the XRD reciprocal space map (RSM) scans in the (1 0 $\bar{1}$ 5) direction, of as-grown, and 1 min GC annealed S1 samples at 790 °C, 910 °C and 1030 °C. The dashed lines in Fig. 2(a)–(d) are drawn through the center of the GaN peaks in the RSMs for comparison to those of the AlInN peaks and indicate relaxation of the AlInN films. Fig. 2(a) indicates that the as-grown AlInN film is grown pseudomorphically on top of GaN (peaks are horizontally in-line), with clear and symmetric circular peaks indicating the high quality of the S1 sample. The RSM for the 790 °C annealed S1 sample in Fig. 2(b) shows no significant loss of signal, indicating that the sample is extremely stable when re-exposed to its growth temperature. Similarly, Fig. 2(c) and (d) show that at 910 °C and 1030 °C annealing temperatures, respectively, the samples retain their pseudomorphic nature and exhibit no additional broadening stemming from potential relaxed parts of the AlInN layer. However, from Fig. 2(d) it can be observed that there is a subtle distortion of the AlInN peak from circular to oval, suggesting that there could be a more pronounced loss of surface indium compared to the other annealing temperatures investigated. Thus, similar to the observations in Fig. 1, it can be concluded that the bulk of the S1 AlInN layer remains pseudomorphic to GaN for temperatures up to 1030 °C, while retaining the high crystalline quality for temperatures well above the growth temperature (~790 °C).

To gain a better understanding of the surface related changes for the S1 samples, AFM scans are performed as shown in Fig. 3. Fig. 3(a)–(d) show 1 μm × 1 μm AFM scans for an as-grown S1 sample, and the GC annealed S1 samples at 790 °C, 880 °C and 1030 °C. In Fig. 3(a), the as-grown S1 sample exhibits a relatively smooth surface with only a few pits and the typically observed circular mounds. The root-mean-square (RMS) roughness is ~0.36 nm, which represents a high surface quality for the ~75 nm thick AlInN film. Fig. 3(b) shows the S1 sample after being re-exposed to the growth temperature of 790 °C, and it can be observed that the surface morphology is beginning to transform with the emergence of smaller closely packed circular grains (~10–25 nm diameter) that are within the original surface morphology. In Fig. 3(c), the original surface morphology is more difficult to identify and the newly formed circular grains from Fig. 3(b) are prominent. Fig. 3(d) shows complete transformation of the surface to a network of closely

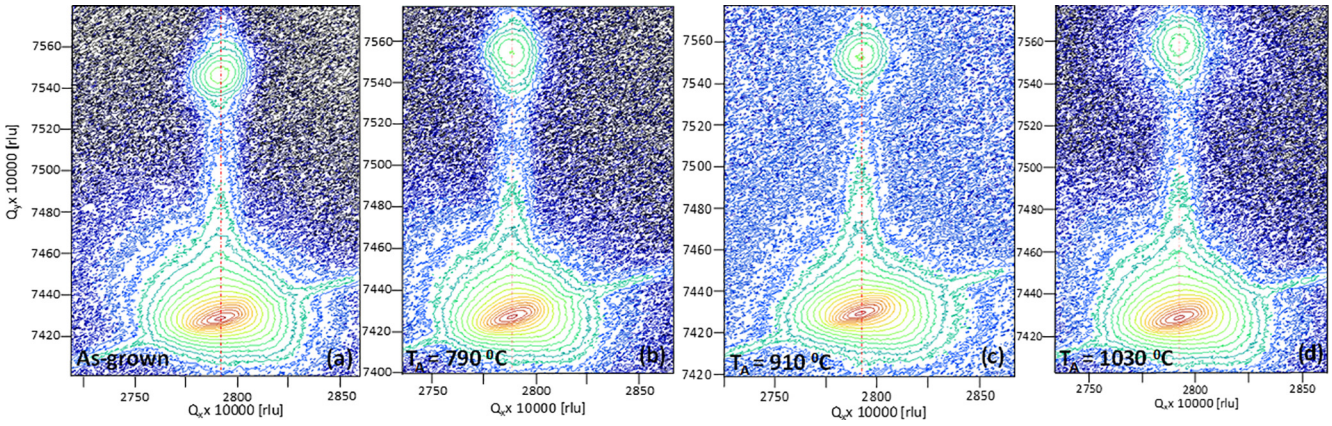

Fig. 2. XRD reciprocal space map scans in the (1 0 $\bar{1}$ 5) direction for an (a) as-grown S1 sample and 1 min GC annealed S1 samples at temperatures of (b) 790 °C, (c) 910 °C, and (d) 1030 °C.

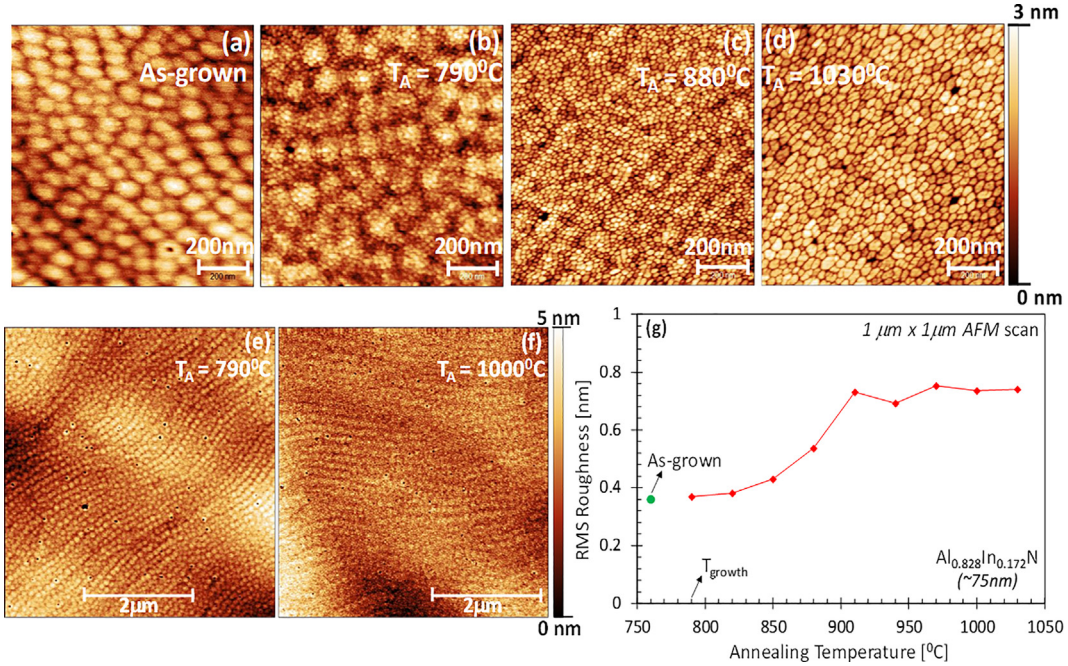

Fig. 3. AFM (1 μm × 1 μm) images for the (a) as-grown and the GC annealed (1 min) S1 samples at (b) 790 °C, (c) 880 °C and (d) 1030 °C. AFM (5 μm × 5 μm) images for GC annealed (1 min) samples at (e) 790 °C and (f) 1000 °C. Plof of (i) RMS roughness as a function of annealing temperature for the S1 samples.

packed oval grains (~40–50 nm in diameter) which is reminiscent of those observed by Sadler et al. [25] and is attributed to surface indium desorption. Similar observations can be made from the 5 μm × 5 μm AFM scans in Fig. 3(e) and 3(f), where the atomic steps became somewhat less recognizable when the annealing temperature is raised from 790 °C to 1000 °C.

Fig. 3(g) shows how the RMS roughness progresses as the GC annealing temperature is increased from 790 °C up to 1030 °C for the S1 samples. For temperatures up to 850 °C, the RMS roughness remains almost unchanged and AFMs of the surface (data not shown) show a similar surface morphology to that of Fig. 3(b), with the RMS roughness reaching ~ 0.41 nm. There is a slight increase in the RMS roughness at 880 °C (~0.54 nm) and 910 °C (~0.74 nm), and then the RMS roughness plateaus at higher temperatures. Hence, contrary to the observations from Figs. 1 and 2, which is a sampling of mainly bulk properties, Fig. 3 shows the very top surface layer is undergoing significant changes at temperatures above 850 °C. It is therefore important to take this into account when designing growth transitions in, for example, multi-layer structures involving AlInN to preserve the overall interface and quality.

4. Section II – Long time annealing study of AlInN

In this section the effect of a long annealing times (120 min) in the XRD on the lattice matched AlInN samples (S2) at temperatures of 850 °C, 950 °C and 1050 °C is studied. Only Gadanecz et al. [29] have previously thermally exposed AlInN to rather long annealing times (30 min) using rapid thermal annealing (RTA) under N_2 atmosphere, compared to all other works where the typical annealing consisted of a "temperature bounce" (1–15 s) at a specific temperature above the typical growth temperature of AlInN (i.e. ~1050 °C) [25–26,28]. Although in a practical scenario the chosen time of 120 min will most likely never be used as a growth transition layer, it is important to understand how the AlInN behaves at elevated temperatures well above the growth temperature for post-growth processes such as thermal annealing to ensure activation of magnesium (Mg) acceptors in p-type layers. Previous demonstrations on p-type AlInN have indicated a significant limitation in hole concentration ($p \sim 3 \times 10^{15}$ cm^{-3}) mostly restricted by the relatively high background of donors and electron concentrations of AlInN alloys (~3×10^{18} cm^{-3}) [10]. Our recent work presents a pathway to increase hole concentrations in AlInN alloys by reducing the background donor doping and electron concentrations by an order of magnitude (~1×10^{17} cm^{-3}) [20]. High hole concentrations in UWBG AlInN would be a significant advancement and would address the low p-type doping of AlGaN alloys for deep-ultraviolet LEDs [31]. However, as in GaN, annealing is most likely required to activate Mg in AlInN, and it is important the AlInN is stable during these longer timed anneals. Additionally, Section II presents results from the XRD anneals where the temperature is "bounced" to a particular temperature and then measured for the XRD DHS scan, which provides essential information on the stability of AlInN when exposed to an N_2 atmosphere at a typical temperature used during GaN growth (i.e. 1050 °C).

Fig. 4(a) shows the ω/2θ (0 0 2) scans of the S2 samples that are GC annealed at temperatures of 850 °C, 950 °C and 1050 °C for 120 min. Note that the baseline of each of the XRD data has been shifted vertically by factors of 10 for improved clarity and comparison. At annealing temperatures of 850 °C and 950 °C the samples exhibit very similar AlInN peaks to that of the as-grown sample as represented by the peaks remaining in close proximity of the vertical dashed line. No additional AlInN peaks are observed for these annealing temperatures which indicates the superb stability of the S2 samples after undergoing an extremely long period (120 min) of high-temperature annealing. On the other hand, Fig. 4(a) shows that the 1050 °C – annealed S2 sample shows significant broadening, coupled with an intensity drop of the AlInN peak which indicates that the sample is experiencing a significant crystallographic change. Additionally, a low-intensity broad shoulder at ~18° can be observed for the 1050 °C-annealed sample in the vicinity of the AlN (0 0 2) peak, suggesting that the indium has begun to desorb from the crystal to form AlN, similar to what has been observed by others [27]. This may in part be caused due to the miscibility gap between the binary constituents, AlN and InN, as calculations of the solubility of this solid have shown that this alloy is unstable in the growth regime studied here [32].

Fig. 4(b) shows the AlInN XRD spectra FWHMs of the S2 samples as a function of annealing temperature (850 °C, 950 °C and 1050 °C) for

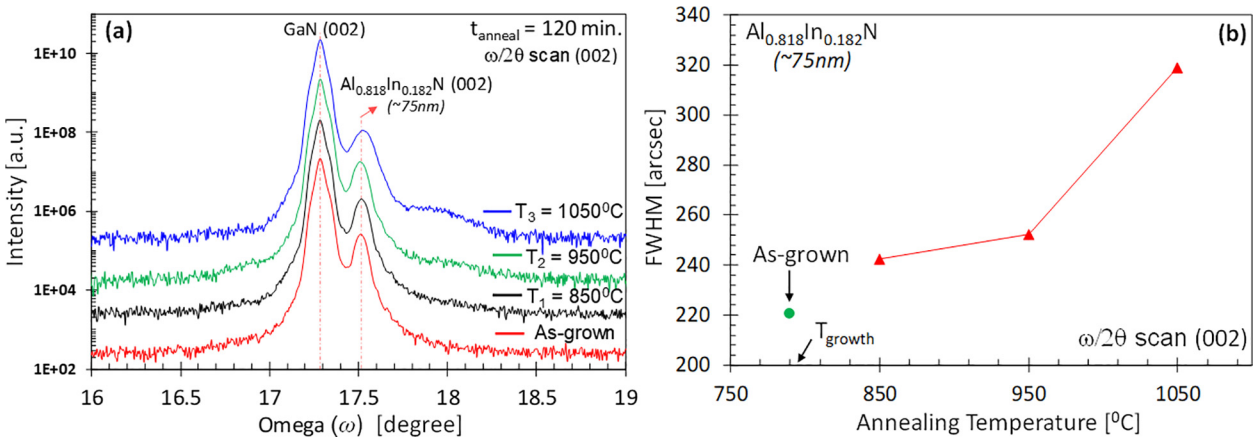

Fig. 4. (a) XRD ω/2θ (0 0 2) scans of S2 samples GC annealed at temperatures of 850 °C, 950 °C and 1050 °C for 120 min, and (b) the AlInN XRD peak FWHM as a function of annealing temperature obtained from the ω/2θ (0 0 2) scans.

the 120-minute-long GC anneals. For temperatures up to 950 °C, the AlInN sample retains the high crystalline quality as the as-grown sample, with a slight (~10%) increase in the FWHM. However, when the S2 samples are exposed to 1050 °C the FWHM increases rapidly by ~ 50% and reaches a value of 320 arcseconds. Such an increase raises the question of whether there are significant changes to the bulk of the AlInN material after the extreme annealing steps. When growing a p-type GaN layer in a typical LED structure, the p-GaN layer is oftentimes annealed at temperatures of ~650–900 °C for ~5–30 min in order to activate Mg-acceptors. Thus, for the case of AlInN, 875 °C is well within the range of temperatures which are suitable for a post-growth Mg activation step. It should be noted, however, that depositing a GaN capping layer was not considered in this study, although previous works [25] have shown its merit to preserve the overall surface and structural quality of AlInN / GaN DBR stacks, which may enable the annealing of AlInN at even higher temperatures than quoted here.

Fig. 5(a)–(c) show AFM (1 μm × 1 μm) scans of the 120 min. GC annealed S2 samples, at temperatures of 850 °C, 950 °C and 1050 °C, respectively. The as-grown S2 sample has a very smooth surface (not shown) with no observed fissures and few pits, and its RMS roughness of ~0.331 nm is similar to that of sample S1 shown in Fig. 3(a). One of the main characteristics of Fig. 5(a)–(c) is the transformation to a network of grains, with the original atomic steps from the as-grown sample completely disappearing. In addition, as the annealing temperature is increased from 850 °C (Fig. 5(a)) to 1050 °C (Fig. 5(c)), the width of the individual grains increases, with some individual grains in Fig. 5(c) having roughly ~4 times the size of those in Fig. 5(a). However, Fig. 5(d) shows that despite the apparent loss of material and the increase in size of the newly-created features, the RMS roughness remains almost completely unchanged, irrespective of the annealing temperature. Namely, the RMS roughness seems to saturate at a value of ~0.9 nm, and it is likely to be dictated by the annealing time rather than the temperature. This is contrary to what is observed in Fig. 3(d), where the RMS roughness of the 850 °C annealed S1 sample remained

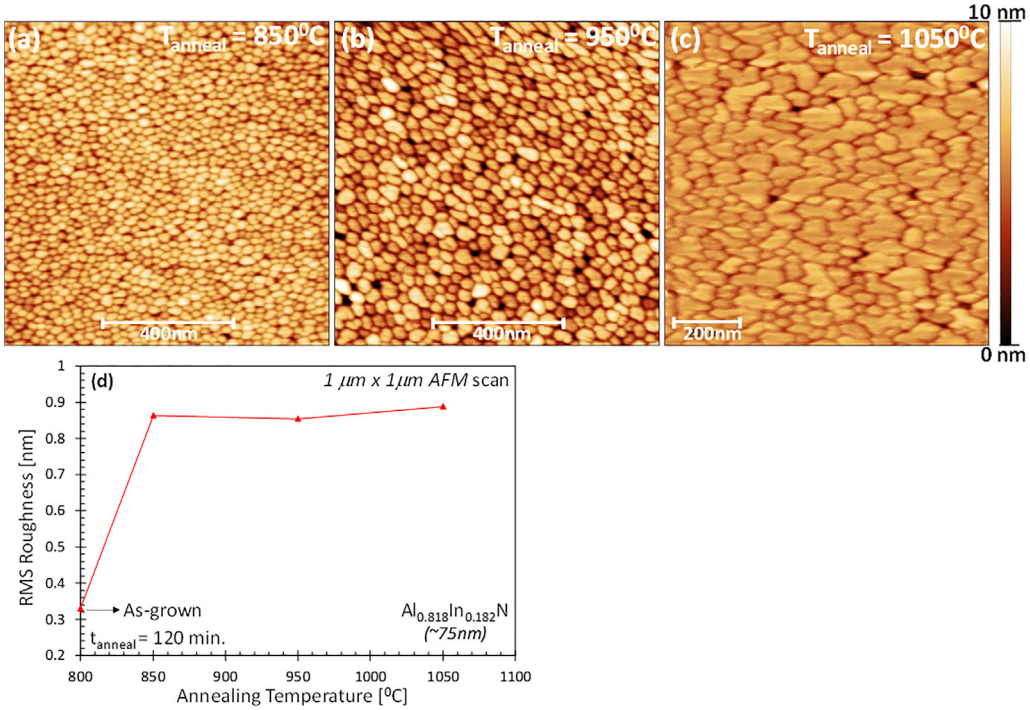

Fig. 5. (a)-(c) AFM (1 μm × 1 μm) images for the S2 samples GC annealed at 850 °C, 950 °C and 1050 °C for 120 min, respectively, and (d) RMS roughness as a function of annealing temperature for the S2 samples.

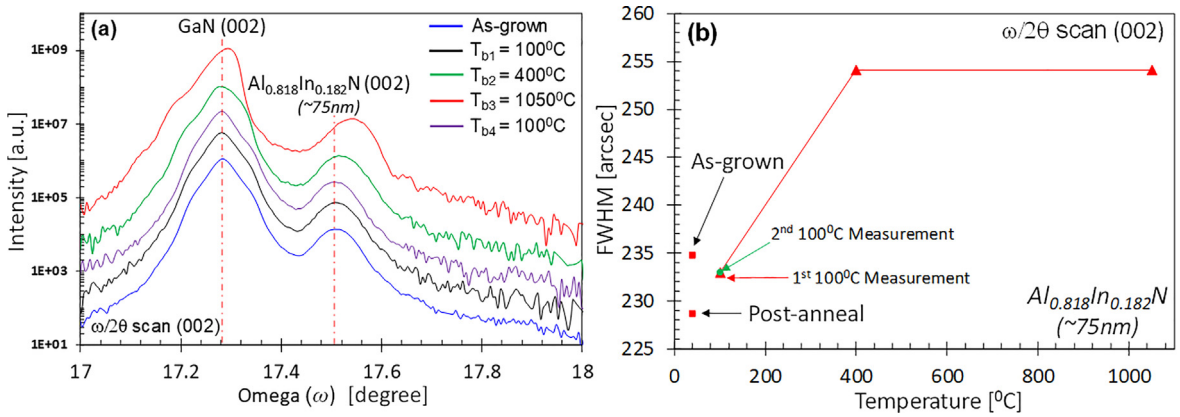

Fig. 6. (a) XRD (0 0 2) scans of an S2 sample during the XRD anneal with a final T_b of 1050 °C and (b) the corresponding FWHM of the sample measured before and after the XRD anneal.

relatively low (~0.41 nm). Understanding of the stability of AlInN under long, high-temperature processing annealings is essential for growth of thick layer structures such as DBRs or thick drift layers in power devices.

Fig. 6 shows the results of the XRD annealed S2 samples with annealing temperatures ranging from 100 °C to 1050 °C, while the as-grown sample is measured at 40 °C. Note that the vertical dashed lines in Fig. 6(a) are drawn through the as-grown S2 samples AlInN peak for reference. The measurements are taken at various "bounce temperatures" (T_b), where the sample was heated to a particular temperature of T_b and then measured in the XRD. There are four temperature sequences (T_{b1}, T_{b2}, T_{b3}, and T_{b4}), with T_{b1} being the first and T_{b4} being the last measurements, respectively. Each measurement is approximately 15 min long and the linear ramping time for reaching the increased target temperature between T_{b1} and T_{b2} is 30 s, while that from T_{b2} to T_{b3} is 2.5 min. The time T_{b3} and T_{b4} is ~25 min and determined by a nonlinear reduction of temperature when turning the XRD heater off. During the measurement, a constant supply of N_2 is ensured to protect the sample surface from potential oxidation, as well as to protect the sample stage from overheating.

The results of bouncing through different measurement temperatures are shown in Fig. 6(a) and indicate whether the sample and overall crystalline quality are recoverable after exposure to thermal cycling in an N_2 atmosphere for temperatures up to 1050 °C (T_{b3}). From Fig. 6(a), changes of the GaN and AlInN peaks are already visible at 400 °C (T_{b2}), while becoming more pronounced at a temperature of 1050 °C. Namely, at T_{b3} both peaks are slightly shifted to a higher angle which suggests that the thermal expansion of both layers is taking place as expected. Assuming a linear dependence of the In-content on the AlInN coefficient of thermal expansion (CTE) and using the values for AlN [33] and InN [34] it was estimated that the value of CTE for GaN [33] is lower than that of the AlInN (~17% In-content), which can explain the larger shift of the omega angle of AlInN peak compared to the GaN peak. When the temperature is lowered back to 100 °C (T_{b4}), the GaN and AlInN peaks regained the identical shape to those obtained from the as-grown and T_{b1} scans, suggesting that the sample has fully recovered after the thermal cycling.

The FWHMs of the S2 sample throughout the XRD annealing measurement are presented as a function of annealing temperature and are shown in Fig. 6(b). At T_{b1}, the FWHM is similar to the as-grown sample (~235 arcsec), while increasing the temperature to T_{b2} and T_{b3} leads to a FWHM of ~255 arcsec, respectively. More importantly, the final scan at T_{b4} shows that the crystalline quality of the sample is retained as the FWHM has reduced back to ~229 arcsec. The AFM data of this sample (data not shown) is also taken after the XRD anneal and the RMS roughness is found to be ~0.416 nm, which is fairly close to that of the as-grown sample (~0.331 nm). Additionally, the AFM image shows that the network of grains did not appear as they did in Figs. 3 and 5, indicating that the grains may originate from the different ambient conditions used during the GC anneals. Investigations of various ambient conditions on the stability of AlInN are not within the scope of this work but will be carried out at a different time. Hence, the temperature bounce XRD anneals shows the resiliency of the AlInN with the ability to preserve extremely high crystal and surface quality which is critical for device processing at temperatures much higher than the growth temperature.

5. Section III – High temperature study of thick AlInN layers

In Section III the results of GC annealing thicker (~275 nm) AlInN samples (S3) at a high temperature (1050 °C) for various times (15–120 min) is presented. The results are compared to the S1 and S2 samples (~75 nm) to understand the influence of thermal exposure for relatively thick nearly lattice matched AlInN films at a typical growth temperature of GaN. In the interest of fabricating high-quality DBR layers using alternating AlInN (~50 nm) / GaN (~50 nm) stacks, the majority of previous AlInN thermal stability studies were focused in thicknesses up to ~ 80 nm [25,28,29]. It has been shown that growth of AlInN on free-standing (FS) GaN can lead to dramatically improved surface quality for "thick" (~300 nm) AlInN layers [35], which will serve as a catalyst to pursue even thicker (> 500 nm) AlInN layers grown via MOVPE for various device applications especially drift layers for power devices [19]. Therefore, coupled with the increased efforts to develop high quality free-standing (FS) GaN substrates for next-generation devices [36], it is important to begin developing an understanding of the temperature limits of AlInN alloys grown on GaN for novel heterostructure designs.

Fig. 7(a) shows the ω/2θ (0 0 2) scans of as-grown and 15, 30, 60 and 120-minute GC annealed S3 samples, respectively. The as-grown sample has a sharp and distinctive AlInN peak with no indication of phase-separation. Similarly, all the annealed S3 samples showed no significant changes in the overall shape in the obtained XRD data, suggesting that the bulk of the AlInN film remained completely unchanged irrespective of the annealing time. Fig. 7(b) presents the FWHM of the S3 samples as a function of annealing time, and it can be observed that the FWHM is virtually unaffected by the increase in the annealing time at a much higher temperature (1050 °C) than the growth temperature (785 °C). It is possible that there are changes in the surface of the S3 sample and the stable results are due to averaging effects in thicker layers, as compared to the S1 sample which is ~4 times thinner. It could also mean that the change at the surface is confined to a very thin layer (~1–2 nm) and that the majority of the bulk sample is extremely stable, even for an "extreme" (120 min) annealing time.

The RSMs for the as-grown and the 120-minute GC annealed S3

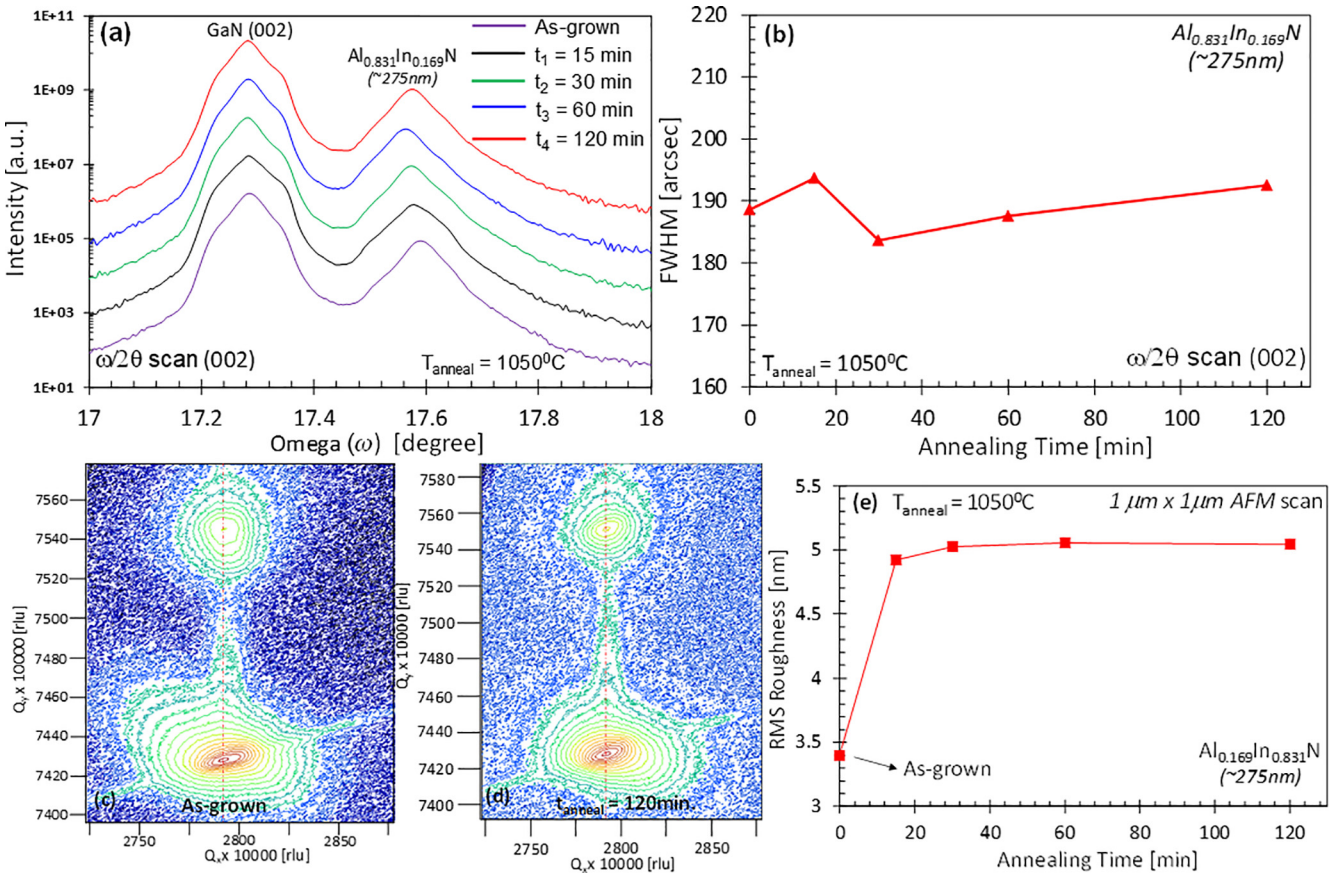

Fig. 7. (a) XRD ω/2θ (0 0 2) scans of S3 samples GC annealed at a temperature of 1050 °C for 15, 30, 60 and 120 min, and (b) their FWHM as a function of annealing time. (c)-(d) XRD RSM scans of as-grown and 120-minute GC annealed S3 samples and (e) the RMS roughness as a function of annealing time for the S3 samples.

samples taken in the (1 0 $\bar{1}$5) direction are shown in Fig. 7(c) and (d), respectively. After 120 min of exposure to a temperature of ~250 °C above the growth temperature, the S3 samples remain pseudomorphic and are still of high crystalline quality, as shown in Fig. 7(d). This result can be confirmed by the relatively comparable RSM signal intensity for the AlInN peaks for both the as-grown and the GC annealed samples. The surface-related changes for the S3 samples are also investigated by means of AFM and the results are presented in Fig. 7(e), where the RMS roughness is plotted as a function of annealing time. The as-grown S3 sample has an RMS roughness of ~3.4 nm, which is typical for thick (~300 nm) AlInN films grown on GaN (on sapphire). The higher RMS roughness in the thicker film is primarily caused by the propagating defects arising from the underlying GaN layer [37], and the complex formation mechanism of a rough upper AlInN layer due to the various effects of V-defect-related phenomena [38] which makes it more difficult to compare to the thinner samples. Surprisingly, increasing the annealing time beyond 15 min seems to have almost no effect on the RMS roughness, as it saturates at about ~5 nm, similar to the trends observed in Figs. 3 and 5. Considering that the RMS roughness of ~5 nm is close to the values reported for AlInN grown on GaN (on sapphire) [39], the overall stability of the AlInN with a thickness of ~275 nm is extremely high for both high temperatures and long annealing times. Thus, it should be noted that the thermal stability investigations presented here are not necessarily representative for the case of AlInN grown on FS GaN substrates, but rather present a potential indicator as to how AlInN on FS GaN may behave at large thicknesses (> 250 nm).

6. Conclusions

Thermal stability investigations of nearly-lattice-matched AlInN films (to GaN) grown via MOVPE were shown. By performing a series of experiments where the AlInN thickness, annealing temperature, and annealing time were varied, the effects on the crystalline quality and surface-related changes were studied by means of XRD and AFM. The importance and understanding of the behavior of thermally treated AlInN alloys were discussed and comparisons were drawn to previous reports. In particular, the nearly lattice matched AlInN showed excellent crystalline stability for temperatures ~250 °C above their typical growth temperature, while surface-related changes became apparent at temperatures of ~850 °C. This work is a detailed investigation of the thermal stability limits of AlInN films with varying thicknesses and will help guide future experiments that require integration of these layers into complex device heterostructures (i.e. as DBR in vertical-cavity lasers, power devices, or laser diodes).

Declaration of Competing Interest

The authors declare that they have no known competing financial interests or personal relationships that could have appeared to influence the work reported in this paper.

Acknowledgments

The work is supported by US National Science Foundation (DMR 1505122, DMR 1708227, and DMR 1726395), and the Daniel E. '39 and Patricia M. Smith Endowed Chair Professorship Fund.

References:

[1] S. Nakamura, G. Fasol (Eds.), The Blue Laser Diode, Springer-Verlag, Berlin, 1997.
[2] H.H. Harima, Properties of GaN and related compounds studied by means of Raman

scattering, J. Phys.: Condens. Matter 14 (2002) R967–R993.
[3] G. Zeng, C.K. Tan, N. Tansu, B.A. Krick, Ultralow wear of gallium nitride, Appl. Phys. Lett. 109 (2016) 051602.
[4] M.H. Crawford, LEDs for solid-state lighting: performance challenges and recent advances, IEEE J. Sel. Top. Quantum Electron. 15 (2009) 1028–1040.
[5] V. Cimalla, J. Pezoldt, O. Ambacher, Group III nitride and SiC based MEMS and NEMS: materials properties, technology and applications, J. Phys. D: Appl. Phys. 40 (2007) 6386.
[6] U.K. Mishra, L. Shen, T.E. Kazior, Y.F. Wu, GaN-based RF power devices and amplifiers, Proc. IEEE 96 (2008) 287.
[7] J. Kuzmik, Power electronics on InAlN/(In)GaN: Prospect for a record performance, IEEE Elect. Dev. Lett. 22 (2001) 11.
[8] J.Y. Tsao, et al., Ultrawide-bandgap semiconductors: research opportunities and challenges, Adv. Elect. Mater. 4 (2017) 1600501.
[9] J.-F. Carlin, C. Zellweger, J. Dorsaz, S. Nicolay, G. Christmann, E. Feltin, R. Butté, N. Grandjean, Progresses in III-nitride distributed Bragg reflectors and microcavities using AlInN/GaN materials, Phys. Stat. Solidi (b) 242 (2005) 11.
[10] Y. Taniyasu, J.-F. Carlin, A. Castiglia, R. Butté, N. Grandjean, Mg doping for p-type AlInN lattice-matched to GaN, Appl. Phys. Letters 101 (2012) 082113.
[11] K. Ikeyama, et al., Room-temperature continuous-wave operation of GaN-based vertical-cavity surface-emitting lasers with n-type conducting AlInN/GaN distributed bragg reflectors, Appl. Phys. Exp. 9 (2016) 10.
[12] G.Y. Liu, et al., Metalorganic vapor phase epitaxy and characterizations of nearly-lattice-matched AlInN alloys on GaN / sapphire and free-standing GaN substrates, J. Cryst. Growth 340 (2012) 66–73.
[13] M. Peart, X.L. Wei, D. Borovac, W. Sun, N. Tansu, J.J. Wierer Jr., Thermal oxidation of AlInN for III-nitride electronic and optoelectronic devices, ACS Appl. Electron. Mater. 1 (2019), https://doi.org/10.1021/acsaelm.9b00266, July.
[14] E. Kohn, F. Medjdoub, InAlN – A new barrier material for GaN-based HEMTs, in: Proc. 14th Int. Work. Phys. Semic. Dev., IWPSD, 6, 311-316 (2007).
[15] Q. Fareed, A. Tarakji, J. Dion, M. Islam, V. Adivarahan, A. Khan, High voltage operation of field-played AlInN HEMTs, Phys. Status Solidi Curr. Top. Solid State Phys. 8 (7–8) (2011) 2454–2456.
[16] W. Sun, S.A. Al Muyeed, R. Song, J.J. Wierer Jr., N. Tansu, Integrating AlInN interlayers into InGaN/GaN multiple quantum wells for enhanced green emission, Appl. Phys. Letters 112 (2018) 201106.
[17] J. Zhang, H. Tong, G. Liu, N. Tansu, High-temperature characteristics of seebeck coefficients for AlInN alloys grown by metalorganic vapor phase epitaxy, J. Appl. Phys. 110 (2011) 4.
[18] Y. Sakai, T. Morimoto, T. Egawa, T. Jimbo, Metal organic chemical vapor deposition growth and characterization of alinn-based schottky ultraviolet photodiodes on aln template, Jpn. J. of Appl. Phys. 50 (2011) 01AD01.
[19] M. Peart, N. Tansu, J.J. Wierer Jr., AlInN for vertical power electronic devices, IEEE Trans. on Elec. Devices 65 (2018) 10.
[20] W. Sun, D. Borovac, M. Peart, J. J. Wierer Jr., N. Tansu, "Low background doping in AlInN films grown via MOVPE", In preparation.
[21] J.-F. Carlin, M. Ilegems, High-quality AlInN for high index contrast Bragg mirrors lattice matched to GaN, Appl. Phys. Letters 83 (2003) 668.
[22] J.-F. Carlin, J. Dorsaz, E. Feltin, R. Butté, N. Grandjean, M. Ilegems, Crack-free fully epitaxial nitride microcavity using highly reflective AlInN/GaN Bragg mirrors, Appl. Phys. Letters 86 (2005) 031107.
[23] E. Feltin, J.-F. Carlin, J. Dorsaz, G. Christmann, R. Butté, M. Laügt, M. Ilegems, N. Grandjean, Crack-free highly reflective AlInN/AlGaN bragg mirrors for UV applications, Appl. Phys. Letters 88 (2006) 051108.
[24] G. Cosendey, J.-F. Carlin, N.A.K. Kaufmann, R. Butté, N. Grandjean, Strain compensation in AlInN/GaN multilayers on GaN substrates: applications to the realization of defect-free Bragg reflectors, Appl. Phys. Letters 98 (2011) 181111.
[25] T.C. Sadler, M.J. Kappers, R.A. Oliver, Optimisation of GaN overgrowth on InAlN for DBRs, Phys. Status Solidi C 6 (2009) S666–S670.
[26] H.R. Brice, T.C. Sadler, M.J. Kappers, R.A. Oliver, The effect of annealing on the surface morphology of strained and unstrained $In_xAl_{1-x}N$ thin films, J. Cryst. Growth 312 (2010) 1800–1806.
[27] C. Berger, A. Dadgar, J. Bläsing, A. Lesnik, P. Veit, G. Schmidt, T. Hempel, J. Christen, A. Krost, A. Strittmatter, Growth of AlInN/GaN distributed bragg reflectors with improved interface quality, J. Cryst. Growth 414 (2015) 105–109.
[28] T. Aschenbrenner, H. Dartsch, C. Kruse, M. Anastasescu, M. Stoica, M. Gartner, A. Pretorius, A. Rosenauer, T. Wagner, D. Hommel, Optical and structural characterization of AlInN layers for optoelectronic applications, J. Appl. Phys. 108 (2010) 063533.
[29] A. Gadanecz, J. Bläsing, A. Dadgar, C. Hums, A. Krost, Thermal stability of metal organic vapor phase epitaxy grown AlInN, Appl. Phys. Lett. 90 (2007) 221906.
[30] H. Angerer, et al., Determination of the Al mole fraction and the band gap bowing of epitaxial $Al_xGa_{1-x}N$ films, Appl. Phys. Lett. 71 (1997) 1504.
[31] K. Ding, V. Avrutin, Ü. Özgür, H. Morkoç, Status of growth of group III-nitride heterostructures for deep ultraviolet light-emitting diodes, Crystals 7 (2017) 300.
[32] T. Matsuoka, Calculation of unstable mixing region in wurtzite $In_{1-x-y}Ga_xAl_yN$, Appl. Phys. Lett. 71 (1997) 105.
[33] H. Iwanaga, A. Kunishige, S. Takeuchi, Anisotropic thermal expansion in wurtzite-type crystals, J. Mat. Sci. 35 (2000) 2451–2454.
[34] K. Wang, R.R. Reeber, Thermal expansion and elastic properties of InN, Appl. Phys. Lett. 79 (2001) 11.
[35] M. Miyoshi, M. Yamanaka, T. Egawa, T. Takeuchi, A 300 nm thick epitaxial AlInN film with a highly flat surface grown almost perfectly lattice-matched to c-plane free-standing GaN substrate, Jap. J. Appl. Physics 58 (2019) SC1006.
[36] R. Fornari (Ed.), Single Crystals of Electronic Materials – Growth and Properties, Woodhead Publishing, 2019.
[37] Z.L. Miao, T.J. Yu, F.J. Xu, J. Song, L. Lu, C.C. Huang, Z.J. Yang, X.Q. Wang, G.Y. Zhang, X.P. Zhang, D.P. Yu, B. Shen, Strain effects on $In_xAl_{1-x}N$ crystalline quality grown on GaN templates by metalorganic chemical vapor deposition, J. Appl. Phys. 107 (2010) 043515.
[38] G. Perillat-Merceroz, G. Cosendey, J.-F. Carlin, R. Butté, N. Grandjean, Intrinsic degradation mechanism of nearly lattice-matched InAlN layers grown on GaN substrates, J. Appl. Phys. 113 (2013) 063506.
[39] M. Miyoshi, M. Yamanaka, T. Egawa, T. Takeuchi, Microstructure variation in thick AlInN films grown on *c*-plane GaN on sapphire by metalorganic chemical vapor deposition, J. Cryst. Growth 506 (2019) 40–44.